A combination of probabilistic and mechanistic approaches for predicting the spread of African swine fever on Merry Island

Facundo Muñoz, David R.J. Pleydell, Ferrán Jori

Epidemics 40 (2022) 100596

Contents lists available at ScienceDirect

Epidemics

journal homepage: www.elsevier.com/locate/epidemics

A combination of probabilistic and mechanistic approaches for predicting the spread of African swine fever on Merry Island

Facundo Muñoz [a,c,*,1], David R.J. Pleydell [b,c,1], Ferrán Jori [a,c]

[a] CIRAD, UMR ASTRE, F-34398 Montpellier, France
[b] INRAE, UMR ASTRE, F-34398 Montpellier, France
[c] Univ Montpellier, UMR ASTRE, Montpellier, France

ARTICLE INFO

Keywords:
African swine fever
Epidemiology
Bayesian modelling
Markov chain Monte Carlo
Synthetic likelihood

ABSTRACT

Over the last decade African swine fever virus, one of the most virulent pathogens known to affect pigs, has devastated pork industries and wild pig populations throughout the world. Despite a growing literature on specific aspects of African swine fever transmission dynamics, it remains unclear which methods and approaches are most effective for controlling the disease during a crisis. As a consequence, an international modelling challenge was organized in which teams analyzed and responded to a stream of data from an *in silico* outbreak in the fictive country of Merry Island. In response to this outbreak, we developed a modelling approach that aimed to predict the evolution of the epidemic and evaluate the impact of potential control measures. Two independent models were developed: a stochastic mechanistic space–time compartmental model for characterizing the dissemination of the virus among wild boar; and a deterministic probabilistic risk model for quantifying infection probabilities in domestic pig herds. The combined results of these two models provided valuable information for anticipating the main risks of dissemination and maintenance of the virus (speed and direction of African swine fever spread among wild boar populations, pig herds at greatest risk of infection, the size of the epidemic in the short and long terms), for evaluating the impact of different control measures and for providing specific recommendations concerning control interventions.

1. Introduction

African swine fever virus (ASFV) is one of the most virulent pathogens known to affect pigs. It has been devastating pork industries and wild pig populations throughout the world since re-emerging in Europe in 2007 and spreading to Asia in 2018. In 2007 African swine fever (ASF) emerged in the Caucasus and subsequently spread widely, affecting at least eleven other European countries (Viltrop et al., 2021) and establishing a sizeable reservoir among wild boar (WB) populations (Sandra et al., 2020; Taylor et al., 2021). Then, in August 2018 ASF emerged in China, from where it spread into at least twelve Asian countries (Mighell and Ward, 2021). More recently, ASF has emerged on the Caribbean island of Hispaniola, affecting the Dominican Republic (Paulino-Ramirez, 2021) and Haiti (OIE, 2021).

African swine fever has a tremendous capacity to spread across borders and expand into new territories. When ASFV spills over into domestic pig value chains, it can spread extensively through farming networks, impose farm-level mortality of up to 100%, and transmission can persist so long as susceptible individuals remain available (Costard et al., 2013; Sánchez-Vizcaíno et al., 2019). Its original sylvatic cycle in eastern and southern Africa involves *Ornithodoros* soft ticks and various wild *Suidae* including warthogs and bush-pigs (Jori and Bastos, 2009; Penrith, 2009). The virus is highly resistant in the environment (Mazur-Panasiuk et al., 2019), thus fomites are thought to represent a significant transmission route despite technical difficulties in confirming their role (Guinat et al., 2016). Moreover, there are currently no available vaccines.

Considering the extraordinary capacity of the virus to invade new territories, there is an urgent need for mathematical models that can realistically simulate the spread of the disease among domestic and wild pig populations, predict potential dissemination scenarios and evaluate the impact of potential control measures (Hayes et al., 2021). In the context of ASF spread in the EU, modelling has helped improve our understanding of ASF dynamics in WB and domestic pig populations. Numerous models have been produced to predict the spread of ASF within and between domestic pig farms (Hayes et al., 2021). Although less abundant, several models have also shown the importance of

* Correspondence to: Cirad, Campus international de Baillarguet, TA A-117/E (E-203), 34398 Montpellier Cedex 5, France.
E-mail addresses: facundo.munoz@cirad.fr (F. Muñoz), david.pleydell@inrae.fr (D.R.J. Pleydell), ferran.jori@cirad.fr (F. Jori).
[1] Contributed equally to this work.

https://doi.org/10.1016/j.epidem.2022.100596
Received 27 October 2021; Received in revised form 10 June 2022; Accepted 13 June 2022
Available online 25 June 2022

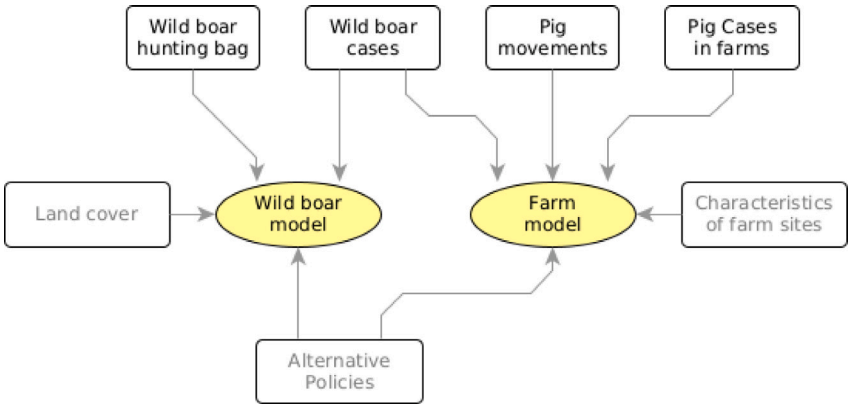

Fig. 1. Data inputs of two models used for inference and prediction during the African Swine Fever Challenge. The inputs for any one model were kept independent of the outputs from the other. Bayesian and frequentist inference was used for the wild boar and pig farm models respectively.

habitat suitability and environmental factors – including infected WB carcasses – to predict the risk of introduction and spread of ASF in WB populations (Pepin et al., 2020; Halasa et al., 2019; Lange and Thulke, 2017; O'Neill et al., 2020) or to compare different control strategies, such as active and passive surveillance for WB carcasses (Gervasi et al., 2019; Gervasi and Guberti, 2021). Despite this prolific scientific production, many knowledge gaps remain. An important shortcoming is that many of those models are limited in their context of application. Most of them have been built on information from Eastern European countries (Baltic countries, Poland), where WB carcasses can function as persistent ASF reservoirs over long cold winters, thus their application to more temperate or tropical regions may be limited. Another major knowledge gap is that, to date, most models are adapted either to the domestic pig cycle or to free-ranging WB populations. However, models addressing the transmission of ASF virus at the interface between domestic and wild pigs are still missing from the literature (Hayes et al., 2021). Finally, another major limitation is the dearth of models that can identify optimal combinations of various control methods so that decision makers may select cost-effective intervention strategies.

This work describes models developed in response to a hypothetical ASF outbreak in a fictive territory (Merry Island) within the context of a modelling challenge (Picault et al., 2021). During this ASF Challenge, teams were provided *in silico* data at three points in the epidemic (day 50, day 80 and day 110 after detection of the index case), demarcating three *phases* of the challenge. Teams used this information to make predictions of the epidemic's evolution, and to evaluate the effectiveness of a number of intervention strategies over the following weeks and months. Here we describe two models designed and implemented in response to this challenge, provide an overview of our main results and predictions, and discuss the implications of this work in the context of ASF control.

2. Methods

The following two models were developed to analyze data from the ASF Challenge:

1. A stochastic mechanistic space–time compartmental model for characterizing ASF transmission dynamics within WB populations (called WB model).
2. A deterministic probabilistic risk model for quantifying the probability of infection and detection of ASF within pig herds given three potential transmission routes (called farm model).

The two models used different sources of information, different geographical representations of cases, and different paradigms of inference (Fig. 1). The parameter estimates and predictions of each model remained independent during the three phases of the challenge.

2.1. Data

The simulated outbreak occurred in the fictive country of Merry Island, an insular territory of 144,209 km^2 located in the Atlantic Ocean, several hundred kilometres from the Azores archipelago (Picault et al., 2021).

Table 1 provides an overview of the data provided at each phase of the challenge. A land cover map indicated that the landscape of Merry Island was composed of agricultural (57%), urban (4%) and forest (39%) areas. Local information indicated that WB (*Sus scrofa*) had an 80% preference for forest habitat, and a expected population size (within each administrative area) of twice the number of WB hunted in 2019. Domestic pig production was represented by 4540 registered pig herds at the beginning of the challenge, distributed in peri-urban (5%), forested (10%) and agricultural (85%) areas. Those herds included commercial (78%) and non-commercial (22%) farms, with outdoor (24%) or indoor (76%) facilities, and breeder (10%), finisher (60%) or breeder/finisher (30%) herds. The data also reported all known between-farm movements of pigs starting two months before the detection of the first ASF case, the spatio-temporal coordinates of detected farm outbreaks, a list of the detected WB cases, and written descriptions of implemented or proposed control measures to contain the epidemics.

2.2. Mechanistic modelling of transmission dynamics within WB populations

Since ASF has a incubation period of several days, we adapted a classic $SEIR$ (susceptible, exposed, infectious, recovered) epidemiological model to simulate spread among WB. Each WB was assumed to inhabit a single hexagonal pixel. Movements of WB were not simulated explicitly, but transitory displacements into adjoining pixels were assumed when calculating infection rates.

For living WB we considered four different health statuses: susceptible (S); exposed (E); infectious (I); and recovered (R) (Fig. 2). Dead WB were assigned to one of two statuses: infectious carcasses (C); and carcasses that were sufficiently decomposed (rotten) to be non-infectious (R_C). Five compartments accounted for the various observation types: hunted WB that were either *untested*, or tested and (correctly) identified as either ASF *positive* or *negative*; and additional infectious carcasses detected via *passive* or *active* surveillance.

For simplicity and computation speed, the WB model: (i) neglected background demographic (birth, death) processes; (ii) assumed WB lived and died (either from hunting or ASF) in the same pixel; (iii) neglected explicit simulation of WB movement between pixels; (iv) assumed that infectious contacts were possible during transitory visits to neighbouring pixels; (v) neglected all contacts between WB from

Table 1
Data provided and questions asked by the challenge organizers at each phase of the African Swine Fever Challenge.

Data provided	Predictions requested
Phase 1: day 50	
• Description of the study area • Data and description of index case (day 0). • Commercial movements of pigs between farms. • Number and distribution of infected and detected pig herds. • Number and distribution of detected WB carcasses including: hunted, tested and infected; hunted, tested and not infected; carcasses found by hikers and hunters; infected found by active search. • Coordinates of proposed fence.	• Number and location of outbreaks in farms and WB cases in the 4 weeks following day 50. • Effectiveness of fencing in the infected forest zone. • Advise on the relevance of implementing increased hunting pressure in the fence area.
Phase 2: day 80	
• Updated epidemiological information on day 80. • Summary of intervention measures on day 80.	• Prediction update on the number of cases in pig herds and WBs. • Effectiveness of 5 potential control strategies compared to the baseline scenario: – Culling all pig herds in the protection zone. – Increase of active search from 1 to 2 km. – Culling all pig herds 3 km around positive WB carcasses. – Increase of surveillance zone from 5 to 10 km. – Culling all herds that traded pigs with infected farms.
Phase 3: day 110	
• Updated epidemiological information Summary of intervention measures • Effectiveness of the fences implemented with or without hunting pressure.	• Status of epidemic at day 230 (potential second wave, endemicity, epidemic-extinction, etc.)

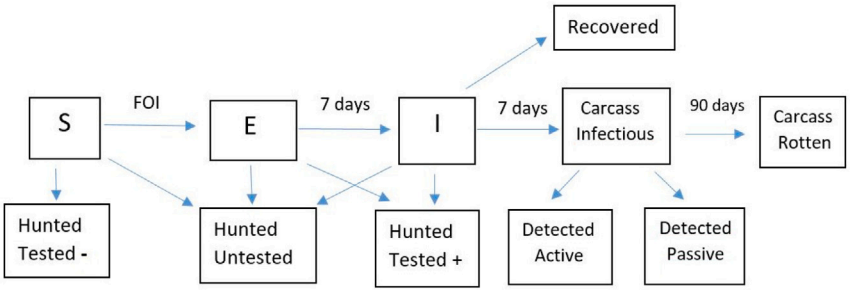

Fig. 2. Compartmental model for ASF spread in WB. For each pixel, the force of infection (FOI) was calculated as a function of the number of infectious WB and infectious carcasses in the pixel and all adjoining pixels (Eq. (2)).

non-adjacent pixels. We also ignored the possibility of hunting and testing recovered (R) WB.

During each phase of the challenge a two-step approach to numerical calculation with the WB model was adopted, whereby (i) available data were used to obtain approximate Bayesian estimates for parameters, and (ii) those parameter estimates were subsequently used in simulations designed to assess and compare different control measures of epidemic control. We hereafter use *estimation* and *prediction* to refer to these two steps respectively. Fixed and determined parameters are reported in Table 2, and estimated parameters and their priors are reported in Table 3.

2.2.1. Spatial representation, land cover and population density

A hexagonal grid was generated across the island with a distance of 5 km between the centroids of neighbouring pixels. The area of each pixel was approximately 21.7 km^2. This scale was esteemed to provide a reasonable compromise between (i) being small enough to characterize localized transmission arising from WB territoriality, and (ii) not being so small that computation time would explode to impractical time scales. For parameter estimation, we used sub-grids corresponding to 20 km rectangular buffers around all known WB cases — this resulted in grids of 402, 613 and 715 pixels for the three phases of the challenge respectively. For prediction, we used the full grid of 6652 pixels.

Proportional cover of each land cover class (forest, agriculture, urban) was calculated within each pixel. These were used to estimate the expected density of WB per pixel, assuming that: (i) in each administrative area, the total population equalled the 2019 hunting bag; (ii) 80% of those WB were in forest, 20% were in agricultural areas and urban WB were neglected; and iii) the effects of these variables were linear. Thus, in a given pixel k, the expected density of WB (D_k) was determined as

$$E[D_k] = \left(\frac{\omega \times p_{\text{Forest}_k}}{\sum_{k' \in A_k} p_{\text{Forest}_{k'}}} + \frac{(1-\omega) \times p_{\text{Agro}_k}}{\sum_{k' \in A_k} p_{\text{Agro}_{k'}}} \right) H_{A_k} \quad (1)$$

where A_k indicates the set of pixels from the administrative area containing the centroid of pixel k, H_{A_k} indicates the number of WB hunted in 2019 in that administrative area, ω quantifies habitat preference (0.8), and p_{Forest_k} and p_{Agro_k} are the proportional cover of forest and agricultural land within pixel k. We originally multiplied this expected value by two, as suggested by local hunters. However, this resulted in simulations generating approximately twice as many hunted negative cases as were observed. Removing this scaling greatly improved the ability of the model to reproduce the observed data. A map of the expected population density is presented in Fig. 3.

2.2.2. Force of infection, connectivity and fencing

The force of infection in WB (i.e. the expected number of infectious events within a pixel in one time unit) was modelled by combining contributions of both living (I) and dead (C) infectious individuals, both within a pixel and within all adjoining pixels, as follows:

$$\text{FOI}_k = S_k \left[\beta_I \left(c_{I_k} I_k + c_{I_{k'}} \sum_{k' \in N_k} w_{kk'} I_{k'} \right) + \beta_C \left(c_{C_k} C_k + c_{C_{k'}} \sum_{k' \in N_k} w_{kk'} C_{k'} \right) \right] \quad (2)$$

Table 2
Fixed and determined parameters of the WB model. Rates ($\tau_\cdot$ and $\beta_\cdot$) are expressed in units of days^{-1}. The deterministic relation shown for τ_A and τ_P applies to challenge phase one only, otherwise see Table 3.

Par.	Description	Value	Source
ω	Preference for forest	0.8	ASFC documentation
p_{Rec}	Probability to recover	1/20	Gallardo et al. (2017)
p_{Test}	Prob. test hunted animal	1/5	ASFC documentation
β_I	Transmission rate (infectious)	$\beta\, p_{\text{Attract}}$	Assumed
β_C	Transmission rate (carcass)	$\beta\,(1-p_{\text{Attract}})$	Assumed
τ_I	Incubation rate	1/7	ASFC documentation
τ_C	Induced mortality rate	1/7	ASFC documentation
τ_{Rec}	Recovery rate	$\tau_C\, p_{\text{Rec}}/(1-p_{\text{Rec}})$	Assumed
τ_{Rot}	Carcass decontamination rate	1/90	ASFC documentation
τ_H	Daily hunting rate	$\frac{-12}{8\cdot 365}\log(1-p_{\text{HuntY}})$	Assumed
τ_A	Carcass detection rate (active search)	$\tau_{\text{Det}}\, p_{\text{Active}}$	Assumed
τ_P	Carcass detection rate (passive search)	$\tau_{\text{Det}}\,(1-p_{\text{Active}})$	Assumed

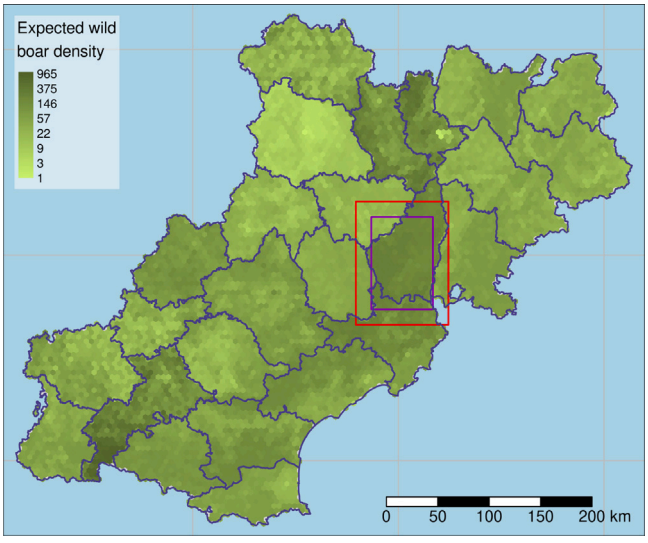

Fig. 3. Expected WB density, as individuals per pixel, across Merry Island. Spatial variation within administrative areas was determined by land cover composition and habitat preference. Discontinuities at administrative boundaries (grey lines) reflect how hunting data where utilized at the district level without smoothing between districts. The inner rectangle represents the fence constructed at the end of day 60. The red rectangle indicates the zone of military intervention (days 61–120).

where S_k is the number of susceptible individuals in pixel k, N_k is the set of adjoined neighbouring pixels, and β_I and β_C scale the rate of transmission from living and dead infectious individuals respectively. The *connectivity coefficients* c_{I_k}, $c_{I_{k'}}$, c_{C_k} and $c_{C_{k'}}$ weight the relative frequency of contacts between a single susceptible and a single infectious-local, infectious-neighbouring, carcass-local or carcass-neighbouring individual. These connectivity coefficients are the probabilities that two individual WB are simultaneously within the same pixel given the probabilities that an individual is in its home or neighbouring pixels at any moment in time (assumed 1 and 0 respectively for carcasses). Thus,

$$c_{I_k} = p_{\text{Home}}^2 + p_{\text{Away}}^2/n_k \tag{3}$$

$$c_{I_{k'}} = p_{\text{Home}}\, p_{\text{Away}} \left(\frac{1}{n_k} + \frac{1}{n_{k'}}\right) + 2\frac{p_{\text{Away}}^2}{n_k\, n_{k'}} \tag{4}$$

$$c_{C_k} = p_{\text{Home}} \tag{5}$$

$$c_{C_{k'}} = p_{\text{Away}}/n_k \tag{6}$$

where $p_{\text{Away}} = 1 - p_{\text{Home}}$ is the proportion of time a WB spends visiting pixels adjacent to their home pixel (the pixel at the centre of their home range), n_k is the number of neighbouring pixels for pixel k. Thus, p_{Away}/n_k is the probability that a WB is visiting a given neighbouring pixel.

The weights $w_{kk'}$ (in Eq. (2)) implement the effects of fencing by reducing contact between WB in specific pairs of adjoining pixels. For most pairs of adjoining pixels $w_{kk'} = 1$. However, following fence completion (on day t_{Fence}), $w_{kk'} = (1 - \omega_{\text{Fence}})$ for all adjoining pixel-pairs with centroids falling on either side of the fence. Thus, an ω_{Fence} of 1 corresponds to 100% fence efficacy (zero transmission).

2.2.3. Parameter estimation

In the estimation step we used Markov chain Monte Carlo (MCMC) to obtain approximate Bayesian estimates for the posterior distribution of the unknown parameters. It is well known that traditional MCMC methods typically perform badly if used to estimate both the parameters and the hidden states of stochastic dynamic models. Particle MCMC methods have been proposed to overcome these limitations (Andrieu et al., 2010), but are not popular for fitting spatial models due to excessive computational overhead. We bypassed these technical limitations by using Monte Carlo simulation to approximate the expected value of a likelihood for a set of data summary statistics. Doing so enabled us to perform MCMC via the adaptive Metropolis–Hastings block sampler provided in NIMBLE (de Valpine and Turek, 2017; de Valpine and Paciorek, 2020). We describe this Monte Carlo likelihood, and how we implemented MCMC, in supplementary sections 2 and 3 respectively.

2.2.4. Simulation

The WB model was defined in continuous time. However, we performed stochastic simulation using the *tau-leap* method — a computationally efficient discrete time approximation to Gillespie's direct method (Gillespie, 2001). We adopted a one-day time step through out, with one exception – the very first time step of each simulation was performed with a shorter time interval of length $\lceil \tau_{\text{Intro}} \rceil - -\tau_{\text{Intro}}$, where $\lceil \cdot \rceil$ represents the ceiling function, which gives the smallest integer greater than or equal to its argument. This was done to avoid discretization of the parameter τ_{Intro}, which may have compromised the performance of the adaptive MCMC algorithm.

At the start of each simulation, the density of susceptible WB in each pixel was drawn from a Poisson distribution with expectancy given by the force of infection (Eq. (1)). Each simulation was initialized at time τ_{Intro}, with a single infectious carcass (C) in the pixel containing coordinates $(x_{\text{Intro}}, y_{\text{Intro}})$. The carcass decontamination rate (τ_{Rot}) was set to 0, until day 0, to limit the frequency of premature stochastic extinction in simulated epidemics.

Stochastic simulation was performed during both the estimation and prediction steps of each analysis. During the estimation step we performed 500, 500 and 1000 simulations per likelihood approximation for challenge phases one, two and three respectively. During the prediction steps, we generated 10000 simulations for each prediction scenario. Each simulation was performed using an independently selected sample of parameters generated in the estimation step (of the given phase).

Table 3
Estimated parameters of the WB model and their priors in each phase. Priors that remained unchanged from the previous phase are omitted. N.A. is displayed in cases where a prior is no longer applicable due to a change in the model. The WB models of phases one, two and three are referred to as WB model 1, 2 and 3 in the main text.

Par.	Description	Prior phase 1	Prior phase 2	Prior phase 3
τ_{Intro}	ASF introduction time	Unif$(-90, 0)$	$-100\times$ Beta$(7, 7)$	
x_{Intro}	Epi-centre easting	Unif$(x_{\min}, x_{\max})$		
y_{Intro}	Epi-centre northing	Unif$(y_{\min}, y_{\max})$		
β	Transmission rate	Exp$(\lambda = 10^{-7})$	Exp$(\lambda = 10^{-1})$	
p_{Attract}	Attractivity of I relative to C	Beta$(1, 1)$	Beta$(2, 2)$	
τ_{Det}	Carcass detection rate	Exp$(\lambda = 10^{-7})$	N.A.	N.A.
τ_{A}	Active search detection rate baseline	N.A.	Exp$(\lambda = 10^{-7})$	
τ_{P}	Passive search detection rate	N.A.	LogNorm$(0, 3)$	
τ_{Phz}	Augmentation of τ_{P} in hunting zone	N.A.	Exp$(\lambda = 10^{-7})$	
τ_{Hhz}	Augmentation of τ_{H} in hunting zone	N.A.	Exp$(\lambda = 10^{-7})$	
p_{HuntY}	Prob. hunted in 1 year	Beta$(330, 330)$		
ω_{Fence}	Efficacy of fence	N.A.	Beta$(2, 2)$	Beta$(1, 1)$
p_{Home}	Connectivity (prob. in home pixel)	Beta$(1, 1)$	Beta$(10, 10)$	$\text{logit}^{-1}(9.8)$
p_{Active}	Relative sensitivity of active search	Beta$(1, 1)$	N.A.	N.A.

2.2.5. Evaluation of predictive performance

Performance of the different WB models was assessed by comparing maps of the *true* cumulative incidence of observed cases with *predictions* (of those values) generated as the mean (per pixel) from 10000 simulations. Observed cases corresponded to all the different ways of detecting infected WB carcasses, given by the model compartments *hunted and positive*, *active search* and *passive search* (Fig. 2). *True* and *predicted* maps were generated for the periods D0-D60 and D0-D110 to evaluate WB model 1 and 2, respectively. Residuals, calculated as the difference between the *true* and *predicted* maps, were checked visually for outliers and unexplained (i.e. non-random) spatial structure. The evaluation of projections issued from WB model 1 was made at day 60, and not at day 80, because the first version of the model did not account for the subsequent increase in hunting pressure.

2.2.6. Evaluation of control strategies

Various control options were evaluated via simulation during the prediction step of each challenge phase. For WB, the principal control interventions were fencing, increased hunting pressure (military intervention), and actively searching for WB carcasses in a given radius around known WB cases.

For simplicity, we assumed that the fence was completely absent up to and including day 60 (t_{Fence}), and became effective at the start of the following day. In the prediction step of challenge phase one, we simulated epidemics with fence efficacy (ω_{Fence}) set to 1.0, 0.98 and zero. For each scenario, the simulated epidemics were used to map the expected cumulative incidence in infectious WB ($E + I$) at days 60 and 80. Here, we extend that initial analysis and assess a more expeditious fence completion by using WB model 3 to simulate 10000 epidemics with t_{Fence} set to day 30, both with and without military intervention.

Challenge phase two provided the first data from which fence efficacy (ω_{Fence}) and the augmentation of the daily hunting rate (τ_{Hhz}) could be estimated — two interventions that were initialized at the end of day 60. We were thereafter able to simulate epidemics using estimates of those parameters, and compare these with simulations where those parameters were set to zero. We also explored the potential benefit of augmenting the radius of the active search from 1 km to 2 km (supplementary materials, section 1).

In challenge phase three, we simulated 10000 epidemics up to day 230, both with and without military intervention, in order to provide a long-term forecast. Military intervention was stopped after day 120. The mean daily value of I from the simulated epidemics was used to approximate the expected long-term trajectory of the epidemic under each control scenario. We also plotted stochastic trajectories of $E + I$ from 1000 simulations, along with the proportion of simulations with $E + I = 0$ at each day, to provide an index of whether or not the epidemic was expected to continue beyond day 230. For each model, the conditional (on emergence) expected day of ASF emergence per pixel was calculated as the mean day on which the first WB of a given pixel became infected — unaffected pixels were omitted from these calculations.

2.3. Probabilistic modelling of transmission among domestic pig sites

A farm contamination model was developed to estimate, for each pig herd on the island, the probability to become infected within a given time period following each data release date. These probabilities accounted for three contamination pathways:

1. direct contact with infectious WB;
2. reception of infected live pigs from animal trade;
3. fomites from neighbouring pig herds.

This model used known locations of pig production facilities as the epidemiological units. We call these *pig production sites*, or *pig sites* for short. We also use the term *pig herds* - although this is only appropriate on sites that have not undergone culling. We rarely refer to *pig farms*, since a single farm may consist of multiple sites. Infection and detection probabilities are considered at the site/herd level. The six key probabilities estimated by the model are presented in Table 4. Fixed parameters are provided in Table 5. All non-fixed parameters were re-estimated during each challenge phase. We used frequentist methods, expected values and point estimates throughout, thereby neglecting uncertainties and errors in parameter estimates.

The model made implicit use of susceptible–infectious–detected–recovered ($SIDR$) compartmental categories to model transmission among pig herds. Each herd was assumed to be within one, and only one, of these compartments on any given day. Non-infected pig herds were all susceptible (S). Any infection starts in category I, where transmission can occur before infection is detected and confirmed after a fixed period of 15 days (thus, all infected pig herds are eventually detected). The infected pig herd then enters category D, for one day, before the herd is culled. The pig production site then remains empty for 50 days, during which time it is considered as recovered (R). Pig sites are disinfected 10 days after culling, during which time transmission via fomites is theoretically possible, although we considered the probability negligible for simplicity. Finally, after re-population, the pig herd becomes susceptible again. While we acknowledge that ASF infection and contamination within domestic pig farms arises from a dynamic process, we do not simulate or track state transitions explicitly. Instead, for each challenge phase, we computed probabilities of each pig-site becoming infected during the prediction period that followed the corresponding data release date, d_j, $j = 1, 2, 3$.

Let $j = 1, 2, 3$ be an index for the days on which data were released to challenge participants, i.e. days 50, 80 and 110 respectively. Let N_j be the number of registered pig herds at the time of data release j. Each pig herd $i = 1, \ldots, N_j$ has 6 associated infection probabilities in each of the upcoming prediction periods (days 51–80, 81–110 and 111–230 for $j = 1, 2, 3$ respectively) that were updated at each challenge phase. These probabilities are described in Table 4

Concerning available data for characterizing pig-sites, two pieces of information were used. First, we considered that only *outdoor* pig herds

Table 4
Key probabilities within the pig-herd model. Sub-indices i and j indicate pig herd and submission phase respectively. The three transmission routes are encoded in the super-indices as: direct contact with WB (wb); contamination via fomites (fm); and infection through the trade of live pigs (tr).

Par.	Description	Value	Source
π_{ij}	**Total infection probability** in the upcoming prediction period	$1-(1-\pi_{ij}^{\text{wb}})(1-\pi_{ij}^{\text{tr}})(1-\pi_{ij}^{\text{fm}})$	Probability of infection by any one of the independently considered pathways
π_{ij}^{wb}	Infection probability due to **exposure to infectious WB** in the prediction period	$1-(1-\pi_{ij}^{d_{\text{wb}}})^{n_{ij}^{d}}$	n_{ij}^{d}: number of days at risk for pig herd i in the prediction period j. See Section 2.3.1.
π_{ij}^{tr}	Infection probability due to **trade** in the prediction period	E_{ij}^{tr}	Approximated by the expected number of infected shipments. See Section 2.3.2.
π_{ij}^{fm}	Infection probability due to **fomites** in the prediction period	$1-\prod_{i'\neq i}\left(1-\pi_{ii'j}^{\text{fm}}\right)$	See Section 2.3.3.
$\pi_{ij}^{d_{\text{wb}}}$	**Daily infection probability** due to exposure to infectious WB during any day in the observed or prediction periods	$1-\left(1-\pi_{ij}^{O_{\text{wb}}}\right)^{n_j^{-1}}$	Values of n_j fixed. See Table 5.
$\pi_{ij}^{O_{\text{wb}}}$	Infection probability due to exposure to infectious WB in the **observed** period. Zero for indoor herds.	$\left[1+\exp\left(-\alpha-\beta e_{ij}^{\text{wb}}\right)\right]^{-1}$	Expected probability from a logistic regression on the exposure to infectious WB for **outdoor herds only**.

Table 5
Fixed parameter values for the pig herd model.

Notation	Parameter	Value	Source
`symptom_onset`	Days from infection to start of clinical signs	7	ASFC documentation. Average value. We considered it constant.
`detection_delay`	Time (days) needed to confirm ASF in a pig herd since infection	15	ASFC documentation. Average value (it actually was 14). We considered it constant.
`day_expo_start`	Day from which the exposition to ASFV started. Start of the *observed period*.	−15	A central value from our simulations of the epidemic among WB.
$d_j,\quad j=1,2,3$	Data release date, in challenge calendar time, at each phase j.	50, 80, 110	Challenge rules.
$n_j,\quad j=1,2,3$	Number of days in the observed period at each phase j.	50, 80, 110	d_j − `day_expo_start` − `detection_delay`
π_{hot}	Probability of transmission for a recent shipment from a suspected pig herd.	0.8	Arbitrarily set as representing a high risk, but with some uncertainty due to chance or mistakes. See Section 2.3.2.

were at risk of ASF contamination via direct contact with infectious WB. Secondly, herd size was used as a quantitative measure of the expected impact of the alternative control strategies proposed by the challenge organizers. We did not use any other farm site characteristics data in the model, since exploratory analyses showed no particular effect of these variables on the six infection probabilities (Table 4).

The pig herd model did not require setting any initial conditions, apart from the fixed parameters listed in Table 5, among which there was the day of disease introduction which represented the beginning of the exposition period. It was set at day −15 in ASF Challenge time, which was a central value from our simulations of the epidemic among WB in phase one. The precise location of the introduction was irrelevant for the pig-herd model as only the area affected by day 50 was used in estimation.

The following subsections describe the methods used for estimating the transmission probabilities of Table 4. These subsections are organized by transmission pathway, namely: contact with infectious WB; trade movements; and transportation of fomites.

2.3.1. Probability of transmission through WB exposure

The exposure of pig herds to infectious WB, e_{ij}^{wb}, was quantified via kernel density smoothing of observed WB case data. This smoothing was performed once for each challenge phase, and was applied to the entire set of available cases — thus temporal fluctuations in the risk of exposure to infectious WB were neglected. We then fitted a logistic regression for the infection status of pig sites given their level of exposure to infectious WB. This allowed the estimation of a probability of *infection and detection*, $\pi_{ij}^{O_{\text{wb}}}$, for each outdoor farm site, pertaining to the entire observation period ranging from the beginning of exposure (`day_expo_start`) up to the `data release date` minus the `detection_delay`. We derived an estimate of the *daily probability of infection*, $\pi_{ij}^{d_{\text{wb}}}$, based on the number of days considered during the observation period, assuming constant risk and independence across time.

The number of days at risk for farm i in the jth prediction period, n_{ij}^{d}, was derived by subtracting the total duration of any known culling/cleaning/
re-stocking periods at that farm site from the length of the prediction period (Table 5). Unknown hypothetical culling/cleaning/re-stocking periods were neglected. This was used, with $\pi_{ij}^{d_{\text{wb}}}$, to obtain an estimate of the *probability of infection from exposure to infectious WB* during the prediction period, π_{ij}^{wb}.

A strong assumption was that only *outdoor* pig herds, with non-negligible exposure, were susceptible to this transmission pathway. Indoor pig herds and farms far from WB cases (i.e. not directly exposed) were excluded from the logistic regression and their value of $\pi_{ij}^{O_{\text{wb}}}$ was fixed at zero, which in turn makes the daily infection probabilities, $\pi_{ij}^{d_{\text{wb}}}$, and the predicted infection probability by WB, π_{ij}^{wb}, also zero.

2.3.2. Probability of transmission through infected shipments

For each pig herd, we calculated the risk of observing an infection within the prediction period due to shipments from infected sources, π_{ij}^{tr}. Any such transmission event must either occur prior to the data release date, in which case the shipment will have been observed, or after the data release date, in which case its occurrence will be unknown. We consider these two contributions separately.

To quantify the probability of an infectious shipment within the observation period, we consider known *recent* shipments occurring within the 15 (`detection_delay`) days before the data release date of each phase (d_j). Earlier shipments were certainly not infectious, otherwise the transmission would have been detected at the destination site prior to the following data release. Among these shipment events, we considered those shipments from farm sites that were *suspected as infected* (but not yet confirmed) in the seven (`symptom_onset`) days following the shipment as particularly risky, and arbitrarily assigned a transmission probability of 0.8 (π_{hot}) to those events. However, we never actually observed this situation in the challenge data. We quantified the transmission risk for the rest of the *recent* observed shipments as the probability of infection of the source site at the day of the shipment. This was done by accumulating its *daily infection probability*, $\pi_{ij}^{d_{\text{wb}}}$, over the number of days at risk from $d_0 = d_j - \texttt{detection\_delay}$ up to the shipment date d_s:

$$1 - \left(1 - \pi_{ij}^{d_{\text{wb}}}\right)^{n_s} \tag{7}$$

where $n_s = d_s - d_0 + 1$. Finally, we computed the *expected number of infected shipments received* as the simple addition of the transmission probabilities of each of the observed recent shipments.

For unobserved future shipments, we evaluated the expected number of infectious shipments as the product of the expected number of shipments in that period multiplied by the probability that a particular shipment is infected:

$$E[\text{inf. ship.}_{i' \to i}] = E[\text{ship.}_{i' \to i}] \cdot P(\text{inf.} \mid \text{ship.}_{i' \to i}). \tag{8}$$

We used the *empirical monthly shipment rates*, $\hat{\lambda}_{i'i}$, scaled by the number of non-banned days in the prediction period, to obtain simple estimates of $E[\text{ship.}_{i' \to i}]$. The probability of a shipment being infectious requires that the infection occurs before the shipment date. Assuming that a shipment can take place any day in the prediction period with equal probability, we marginalize the corresponding joint probability over the day of the shipment, assuming a uniform distribution, where the joint probability of an infected shipment at day t can be evaluated from the daily probability of infection of the herd at the origin and the number of non-banned days in the prediction period $n_{i'j}$.

$$\begin{aligned} P(\text{inf.} \mid \text{ship.}_{i' \to i}) &= \sum_{t=1}^{n_{i'j}} P(\text{inf.} \mid \text{ship.}_{i' \to i}, t)\, p(t) \\ &= \frac{1}{n_{i'j}} \sum_{t=1}^{n_{i'j}} \left[1 - (1 - \pi_{i'j}^{d_{\text{wb}}})^t\right] \\ &= 1 - \frac{1}{n_{i'j}} \frac{1 - \pi_{i'j}^{d_{\text{wb}}}}{\pi_{i'j}^{d_{\text{wb}}}} \left[1 - (1 - \pi_{i'j}^{d_{\text{wb}}})^{n_{i'j}}\right] \end{aligned} \tag{9}$$

The expected number of infected shipments in the prediction period were computed for all target farm sites by adding together the individual expectations from all the possible origins.

In summary, for every target pig herd, i, we obtained expected numbers of infectious shipments from past or future movements. These were added to give a total expectation for the prediction period, E_{ij}^{tr}, that can be considered as the expected value of a binomial variable $X \sim \text{Bin}(n_{ij}, p_{ij})$ for the number of infected shipments. The probability of at least one infected shipment is approximately equal to E_{ij}^{tr} for $E_{ij}^{\text{tr}} < 0.25$,

$$\pi_{ij}^{\text{tr}} = P(X > 0) = 1 - (1 - E_{ij}^{\text{tr}}/n_{ij})^{n_{ij}} \approx E_{ij}^{\text{tr}}. \tag{10}$$

This approximation avoids dependency on the total number of received shipments, n_{ij}, which is uncertain for future shipments.

2.3.3. Probability of transmission through fomites

Contamination via fomites most likely occurs when the virus is transferred on some inanimate matter, prior to detection, from a neighbouring farms. Thus, the probability of infection via fomites must be proportional to the aggregated probability of infection on neighbouring farms, particularly the closest ones. We assumed that the risk for a given pig herd i to become infected with ASF during phase j via the transportation of fomites from some neighbouring farm site i' was proportional to the probability of infection by infectious WB, $\pi_{i'j}^{\text{wb}}$, weighted by an exponentially decaying function of the distance between the sites, $d_{ii'}$:

$$\pi_{ii'j}^{\text{fm}} = \pi_{i'j}^{\text{wb}} \exp(-d_{ii'}/\lambda) \tag{11}$$

where the scaling parameter was chosen as $\lambda = 700/\log(2)$ so that the probability of infection is halved every 700 m. This was calibrated after the first recorded infection of an indoor herd (site ID 2634) during the challenge, which was in close proximity (about 710 m) to an outdoor finishing farm which was identified as being infected during challenge phase two.

Every target site i has multiple neighbours presenting different levels of risk depending on their respective distances and probabilities of infection from WB. Therefore, the risk of infection via fomites from *any* of the neighbours was computed by aggregating their individual risks, assuming that transmission events from neighbouring pig herds are independent, as follows,

$$\pi_{ij}^{\text{fm}} = 1 - \prod_{i' \neq i} \left(1 - \pi_{ii'j}^{\text{fm}}\right). \tag{12}$$

This unavoidable approximation ignores some sources of dependency, such a veterinarians or other vehicles visiting several neighbouring farms, which may result in clustered transmission. Therefore, it is possible that this simplification leads to some underestimation where probabilities of infection are aggregated.

2.3.4. Evaluation of predictive performance

Prediction performance was assessed informally in three ways. First, by comparing predicted infection probabilities for a period against reported infections. Specifically, we verified that predicted probabilities at infected pig herds were relatively high. This procedure led us to introduce the fomites contamination pathway in phase two, in order to explain the contamination of an indoor farm (site ID 2634) which had been predicted as being at very low risk in our phase one analysis. Secondly, the predicted risk and the observed infection status at pig sites were mapped for visual comparison, in order to identify spatial patterns and to gauge the relative proportion of infected sites given their predicted risk. Thirdly, comparing the expected number of infected *pigs* against the observed number.

2.3.5. Evaluation of control strategies and critical trade hubs

Some of the proposed control strategies, such as increasing the hunting pressure or the size of the active search area, only had indirect impacts on farms, through their effects on the epidemic among WB. By contrast, the direct impacts of control measures involving the culling of pig herds meeting specific criteria (located in protection zones; located near infectious WB carcasses; traded pigs with an infected farm in a certain period before detection), were evaluated by modifying the parameters n_{ij}^d, which represent the number of days at risk for a given farm in the prediction period (see Section 2.3.1), and comparing the resulting infections probabilities.

In order to assess long-term risks, we consider the potential of farms to disseminate ASF through the trade network. A measure of this potential is given by the relative contribution of each farm to the basic reproduction number R_0 of the network (Volkova et al., 2010). This parameter allows the identification of farms that are particularly susceptible to spread the virus widely across the trade network, should they become infected. Specific surveillance measures can be suggested to policy makers to prevent infection of these *trade hubs*.

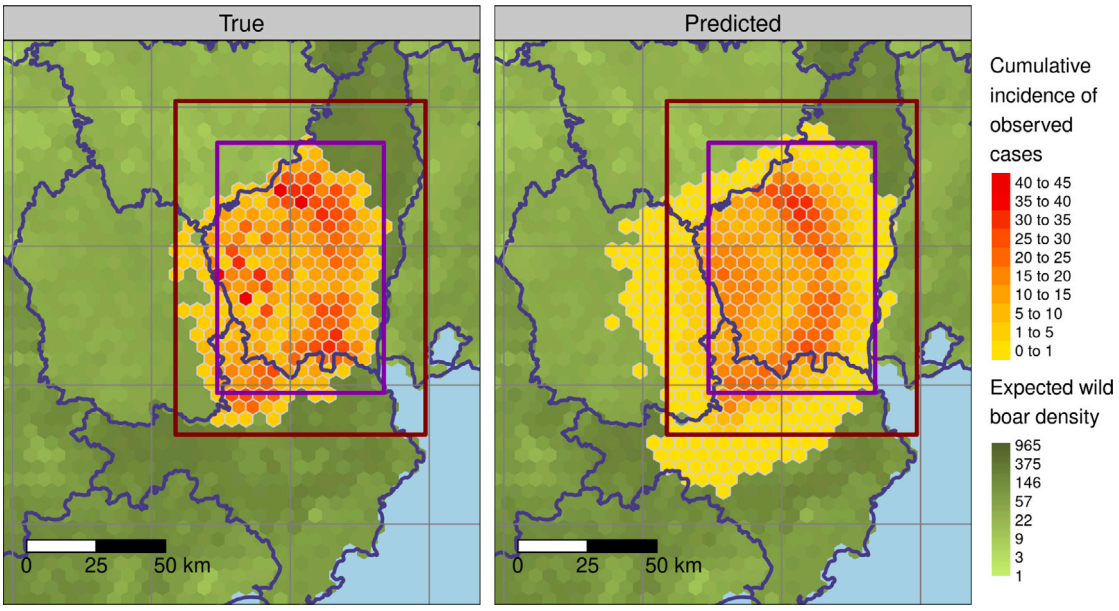

Fig. 4. *True* (left) and *predicted* (right) cumulative incidence of observed WB cases at day 110. The predictions are expected values from 10000 simulations of a model trained on 80 days of data (WB model 2). Rectangles represent the fence (inner) and buffer zone of military intervention (outer). Administrative boundaries are shown in blue.

2.4. Implementation

Our primary language was R (R. Core Team, 2020) and we used 44 CRAN packages — the most critical ones being drake for reproducibility (Landau, 2018), NIMBLE for the WB model (de Valpine and Turek, 2017; de Valpine and Paciorek, 2020), sf for spatial data (Pebesma and Bivand, 2005), knitr for rendering Rmarkdown (Xie, 2020), and tmap for mapping (Tennekes, 2018). Whilst `drake` provides a pipeline for reproducible research (by ensuring every user generates the same *target* R objects), the heavy calculations performed with NIMBLE did not fit within the `drake` framework, thus `drake` and Rmarkdown were simply given access to the outputs of `NIMBLE` scripts. The code, data and reports from each challenge phase are available at https://forgemia.inra.fr/umr-astre/asf-challenge.

3. Results

Here we present key results from the ASF Challenge, including short-term predictions of dissemination among WB and farms, and answers to operational questions about the relative efficacy of alternative control interventions. Additional results are provided in the supplementary document.

3.1. Predictions of spread among WB

We hereafter refer to the models fitted to 50, 80 and 110 days of WB data – in challenge phases one, two and three – as WB models 1, 2 and 3 respectively.

3.1.1. Evaluation of model fit

Fig. 4 compares the *true* cumulative incidence of observed WB cases at day 110 with expected values *predicted* by WB model 2. In general, the expected cumulative observed incidence (right) is smoother than the *true* values (left). Whilst some differences in smoothness were expected due to discrete (left) and continuous (right) representations, this does not account for differences in spatial structure within those areas first affected by the outbreak (near the western fence), where the *true* data exhibits large between-neighbour differences that are absent in the mean of the simulations in that area and in the data from areas further from the epicentre. A map of residuals also exhibits greater levels of local variation in model errors in the areas first affected by the epidemic (Fig. S3). This pattern likely reflects (i) local aggregation in the detection probability due to active searches prior to day 60, and (ii) an augmentation and homogenization of detection probabilities once culling started. That expected values, calculated from 10000 simulations, smoothed over locally aggregated observations is not surprising. Moreover, many features of the *true* data are well characterized by the predictions: such as the extent of the area where the cumulative incidence exceeds one; spatial trends within the main clusters; maximum values of the cumulative incidence; limited dissemination into the administrative areas in the north-west and west of the military area; and considerable leaking of ASF beyond the southern fence. Whilst some simulations did predict more extensive spatial spread than was actually observed (yellow pixels in Fig. 4), the low expected value of the cumulative incidence (<1 observed case) in those areas suggest that the majority of simulations did not support the possibility of spread beyond the southern and western limits of the augmented hunting zone prior to day 110. Maps of the predictions and residuals for WB model 1 provide similar interpretations (Figs. S1 and S2).

The predictive performance of all models developed within the ASF Challenge is assessed in Ezanno et al. (2022). Fig. 2 therein shows that our WB model accurately predicted the dynamics of the challenge organizers simulated epidemic — the trajectory of their M0 model remaining within our 80% credibility intervals throughout the predictive periods.

3.1.2. Effects of control interventions

Simulation was used to explore the effects of fencing, military intervention (augmented hunting pressure) and doubling the active search radius from one to two kilometres. Predictions from WB model 2 indicated that increasing the active search radius to two kilometres would have only negligible impacts on the course of the epidemic (Fig. S4). Indeed, the 95% credibility interval for the proportion of infections caused by carcasses was just (0.00006, 0.015). Expected trajectories for the number of infectious WB (I), with and without fencing and increased hunting, shown that both fencing and military intervention were estimated to reduce the number of infectious WB (Fig. 5). However, the effect was much stronger for military intervention than for fencing alone — the increased hunting pressure having a large immediate effect in reducing infectious WB numbers. Moreover,

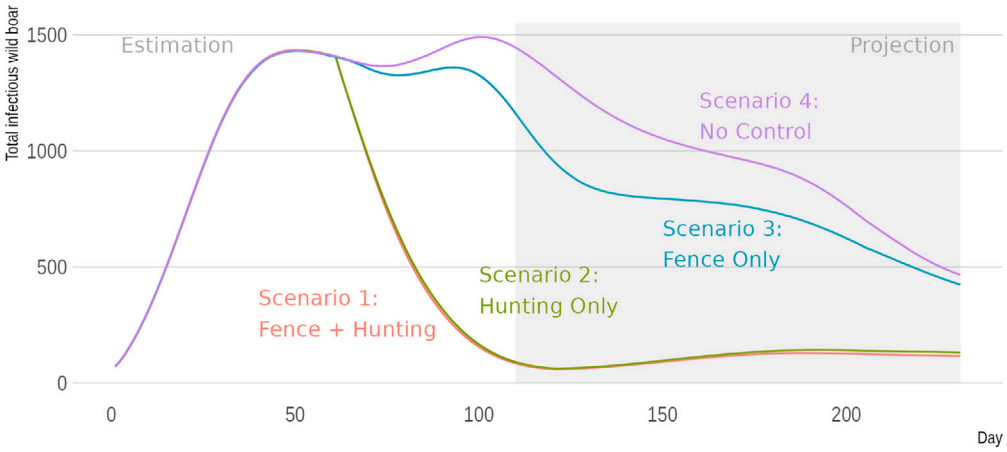

Fig. 5. Trajectories of the expected number of infectious WB (I) by control scenario with data observed up to day 110. These expected values are from WB model 3.

expected trajectories suggest that fencing was unlikely to provide much benefit beyond those of hunting.

Under none of the four control scenarios considered (Fig. 5) was it expected that the epidemic would be brought to a stop. Indeed, the estimated probability of having zero infected ($E+I$) WB at day 230 was approximately 0.4 (Fig. 6). The number of infected WB followed a sharp decline after day 60 in all simulations, however, in only a minority of simulations did it get close to zero and remain there. The majority of simulations suggested that a second wave would start at some point after day 100. Second waves in these simulations arose when ASF escaped through the southern limit of the military intervention zone (Fig. S10). According to WB models 2 and 3, this leaking was expected to occur before days 100 and 120 respectively (Figs. S9 and S10). Simulations from all three models indicated that ASF was expected to have leaked beyond the southern fence prior to its completion on day 60 (Figs. 4, S1, S8, S9 and S10, although see Fig. S11).

Had the fence and military intervention been implemented much earlier, on day 30 for example, the probability of bringing the epidemic to a halt by day 230 would have been much greater (Fig. S5). In that scenario, there is even a non-negligible probability that the fence alone could have stopped the epidemic (Fig. S6). Whilst the most likely value of fence efficacy was very close to one, large uncertainties remained regarding this parameter (Fig. S7). Interestingly, the expected cumulative incidence of infected WB outside the northern and eastern fence remained less than one (salmon-red polygon, Fig. S10), suggesting that in those areas the fence did help limit dissemination. Nevertheless, the large uncertainty in fence efficacy led to the expectation that, without military intervention, the epidemic would have spread beyond the fence in the north and east, and the extent of spread in the south and south-west would have been even greater (Fig. S11).

3.2. Predictions of outbreaks in pig herds

In the first phase of the challenge, three farms (site IDs 4017, 4020 and 737) had a predicted probability of infection and detection remarkably higher than the rest (Table 6) and were indeed infected in the subsequent days. The main risk for the first two farms was their exposure to infectious WB, and it was most likely the actual transmission pathway, whereas farm site 737 was most likely infected via *trade*. In total, 506 pigs were expected to get infected in the first prediction period, from day 51 to day 80. Analogous predictions from challenge phases two and three can be found in Tables S1 and S2 of the supplementary document.

Fig. 7 shows the spatial locations of pig herds with non-negligible ($p > 0.05$) infection probability during each prediction period.

Out of the 4540 pig sites on Merry Island, 411 were associated with trade activities that were sufficiently extensive to risk disseminating the disease throughout the network of farms. Of these, 224 herds accounted for 80% of the *transmission potential* - thus, just 5% of herds accounted for most of the risk of spreading the disease widely through the trade network. These well connected trade hubs can be considered as potential *super spreaders*. Particular attention must be paid to prevent infection at such sites. As the affected area grew larger by day 110 (challenge phase three) four such pig herds were at considerable risk of infection (site IDs 499, 1815, 3796 & 4304, see supplementary Table S2). These were all outdoor facilities, located in vicinity of the southern fence. In the absence of suitable control measures, infection at these sites could have led to dissemination across the entire island.

Table 6
Probability of infection in pig herds without known ASF cases but with non-negligible probabilities ($P > 0.05$) in the period from day 51 to day 80 (phase one of the challenge).

id	size	wb_expo	trade	fomites	p_pred
4017	12	0.383			0.383
4020	5	0.331			0.331
737	1428		0.261	0.006	0.265
2939	664		0.059	0.019	0.077
2960	421		0.059	0.017	0.075
4534	2	0.036		0.031	0.066
1983	131		0.059	0.002	0.060
2955	49			0.055	0.055
1759	536			0.051	0.051
154	8	0.039		0.012	0.051

3.3. Impacts of control on farm outbreaks

With the policy of disease control on farms in place at day 80, the disease was estimated as most likely to continue spreading locally between neighbouring herds within the fenced area and buffer zone. However, the risk of infectious animal shipments out of the area was very low (probability of infection due to trade below 1% for all pig herds) according to our model.

We expected 7180 (out of 4 M heads in total, 0.17%) new pig infections during the second prediction period (days 81–110) under the control strategy in place at that time — namely culling of infected herds and trading ban in protection and surveillance zones. The impacts of the three proposed supplementary control strategies was estimated as marginal, with a maximum reduction of 11 individuals if culling all pig herds located less than three kilometres from positive WB carcasses was applied. This showed that the control strategy implemented on farms during phase two was effective in containing the spread of the disease.

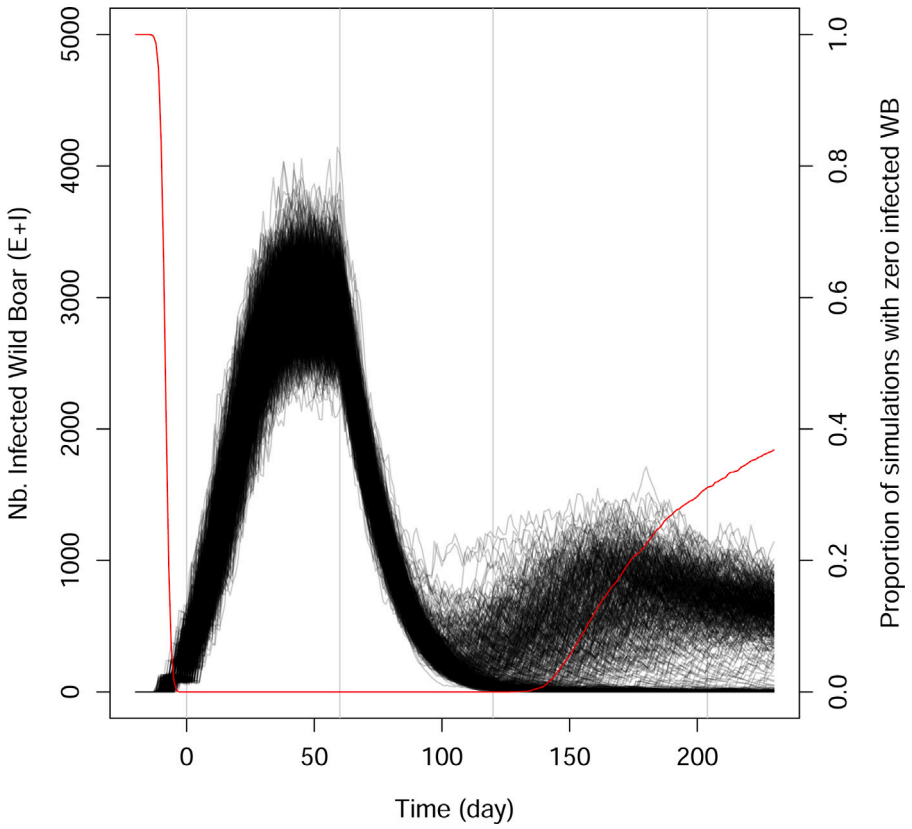

Fig. 6. Stochastic trajectories for the number of infected WB ($E + I$), from simulations with WB model 3. Trajectories from one thousand simulations are shown (black lines) with the proportion of simulations for which $E + I = 0$ (red line).

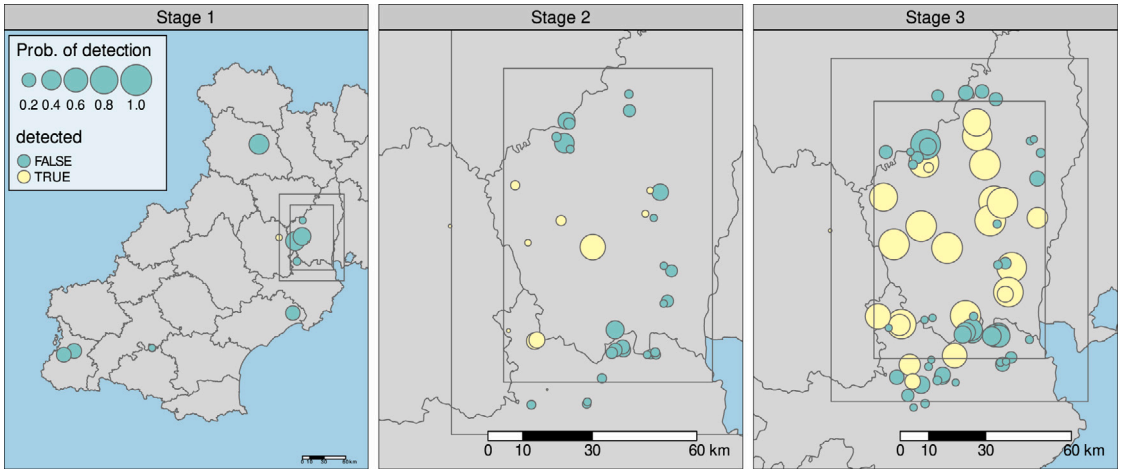

Fig. 7. Probability of outbreak occurrence and detection at farm sites, by any possible pathway, during the prediction period of each phase of the challenge. The rectangles represent the fence (inner) and buffer zone of augmented hunting pressure (outer).

4. Discussion

We have presented a modelling approach that has proved effective for anticipating risks, and for evaluating the impacts of alternative control measures, during the course of an *in silico* ASF outbreak within a fictive country, within the context of a modelling challenge. Our approach was to independently develop a stochastic space–time model of dissemination among WB, and a deterministic probabilistic model for quantifying risks in pig herds. A key advantage of this approach was that it facilitated simultaneous and independent development of the two models, thereby optimizing human resources within a small modelling team working to tight deadlines.

4.1. Model performance and adequacy

Evaluations of model fit indicated a satisfactory level of model performance. During challenge phase one, the three pig sites identified as being at highest risk of infection during the first prediction period (days 51–80) were indeed verified as infected in the subsequent data release. We also accurately predicted that spread among WB would likely be slow and broken to the west of the initial cases, would spread rapidly towards the east and north-east, although probably not beyond the fence, and would pass the fence in the south where a second wave was likely. In challenge phase two, we predicted an expected total number of infected pigs of 6719 — the actual figure at day 110

was 4943. Again, all three pig herds identified as being at highest risk experienced ASF outbreaks in the prediction period preceding the following data release. Moreover, we were able to quantify the impact of proposed control measures in terms of the number of new infections in pigs and the dissemination of the virus among WB populations. This enabled us to provide the decision makers of Merry Island specific recommendations of resource allocation and surveillance activities to limit the spread of the epidemic.

4.2. Limitations and potential improvements of the farm model

Despite integrating three different transmission pathways, the farm model was quite simple and several limitations were apparent. A clear limitation was that predictions were static and simply provided expected values across each prediction period (D51-D80, D81-D110, D110-D230). This lack of dynamics and uncertainty quantification in the predictions could be improved, for instance, by accounting for the progress of the epidemic in WB populations, by adopting a time-to-event approach to model infection risk and by using a parametric statistical model. However, attempts during phase three to link pig herd exposure to predictions of the WB model indicated that identifying an appropriate link was non-trivial — none of the assumed links between the two models that we tested appeared to improve predictive power, thus this line of work was dropped. Secondly, empirically observed between-herd shipment rates were used as probability estimates of future shipments between the same herds. More sophisticated analyses, such as those provided by network analysis models (Ferdousi et al., 2019), could have possibly increased the robustness of the estimates and provided a quantification of their precision. A third potential improvement could be achieved by relaxing the assumptions of independence between the three contamination pathways affecting pig herds. A further improvement could be the replacement of fixed empirical point estimates by full probability distributions. Despite these simplifications, the consistency between model predictions and the reported progress of the disease suggests that the model was nevertheless reasonably robust in predicting the spread of ASF virus through the domestic pig value chain.

4.3. Limitations and potential improvements of the WB model

First, not all of the parameters were independently identifiable. In particular, the very strong correlation between connectivity (p_{Home}) and transmission intensity (β) indicates that, given the available data, we could only achieve low precision in estimating the rate of within-pixel transmission. This prompted us to fix p_{Home} to the median value obtained from a MCMC pre-run in challenge phase three. However, incorporating additional information from secondary sources, such as a strongly informative prior for p_{Home} (based on WB territoriality data, for example), may have helped alleviate this identifiability issue. A second issue was that we unintentionally neglected the hunting of WB in the R compartment. Whilst it was unclear if the diagnostic tests of the challenge would have categorized WB in R as positive or negative, the omission of hunted R from the likelihood was clearly a potential source of bias. However, this bias was surely small if our assumption of 95% diseased induced mortality was reasonable, and the model was most likely flexible enough that it could compensate for this bias and thereby still provide reasonable dissemination estimates. Thirdly, perhaps one of the biggest limitations was to not link the WB model to infection risk in pig farms. This transmission mechanism is expected to be important in real situations, and it is suspected to have played a major role in the maintenance of ASF in areas like Sardinia, the Russian Federation and Romania (Boklund et al., 2020). Finally, our wild boar model assumed density-dependent transmission. This assumption follows the received wisdom that the majority of wildlife diseases are primarily transmitted through density-dependent mechanisms. Indeed, this was the assumption made by the challenge organizers (Picault et al., 2021), and visual inspection of the provided data made it clear that spread was rapid in high-density areas and slow in low density areas — thus the density-dependent assumption was a reasonable choice in the given context. However, some authors have suggested that frequency-dependent mechanisms may also contribute to ASF dynamics (O'Neill et al., 2020), although we do not know of field studies that confirm this proposal. Clearly an expanded statistical framework, that could distinguish between density and frequency dependence, could be advantageous when faced with real data. For example, such an approach has been used to show that, despite the received wisdom, frequency-dependent mechanisms are more important than density-dependent mechanisms in the circulation of mange among wild foxes (Devenish-Nelson et al., 2014).

4.4. Implications for real scenarios and lessons learnt

4.4.1. The role of the density of WB populations

Despite numerous simplifications, the WB model did appear to provide a robust characterization of the speed and extent of spatial spread. This success was largely due to the availability of very detailed information regarding WB densities. Whilst our linear equation for the expected density of WB per pixel (Eq. (1)) might clearly over simplify many real situations, it does appear to have provided a useful approximation to the spatial distribution of WB within the challenge's data generation model. By comparing spread in various directions (e.g. Figs. S10 and S11) with maps of WB density (Fig. 3), we can clearly see that WB densities affect the speed and extent of dissemination. This relation is largely a result of density dependence in the force of infection (Eq. (2)). This relationship explains why ASF was unable to invade the administrative region north of the epicentre in our simulations. If density dependence is indeed the most pertinent mode of transmission, then clearly the quality and quantity of WB data can greatly affect the reliability of estimates concerning the speed and extent of ASF dispersal. The implication of this density~speed relationship for real world applications is that WB densities need to be known across entire landscapes, at least up to a constant of proportionality, for predicting spatial heterogeneity in the spread of ASF among sylvatic reservoirs. Thus, one of the most important aspects when developing predictive models in the context of real ASF epidemics is the quality and quantity of available WB abundance data. However, this typically presents a critical knowledge gap in real world scenarios because WB numbers are extremely difficult to estimate with accuracy in the field.

Wild boar densities have been estimated across continental areas via various combinations of remotely sensed data, spatial analyses and collations of various sets of census and hunting data (Alexander et al., 2016; Sales et al., 2017; Lewis et al., 2017; Bosch et al., 2017; Pittiglio et al., 2018). However, data quality is problematic for such studies, particularly in areas where census data are not available and hunting data must be used as a proxy. It is rare for hunting organizations to report *hunting effort*, an important parameter for interpreting hunt statistics: for example, in France, just two out of the 96 metropolitan departments are routinely reporting hunting effort (Vajas, pers comm), thus large uncertainties surround the calibration of hunting data from multiple administrative areas. Furthermore, numerous methods exist for estimating WB densities in the field, and these vary in their accuracy and reliability (ENETWILD consortium, 2020), therefore available density figures from various countries may not be directly comparable. As such, teams attempting to map WB densities across large areas must typically make various simplifying hypotheses concerning data quality, thus levels of precision remain unknown. These real world errors and uncertainties have important implications for the robustness of predictions from ASF dissemination models built using current WB density maps. This aspect was greatly simplified during the ASF challenge, where hunting and landscape data alone were sufficient for obtaining reliable estimates of WB densities across Merry Island.

4.4.2. The geographical resolution of the analysis

In our simulations, dissemination among WB reached speeds of up to ~ 27 km/month (Fig. S10). This value is much higher than estimates reported in real situations, calculated using data from seven different countries in Western and Central Europe, which range from 2.9 to 11.7 km/month (Podgórski and Śmietanka, 2018; European Food Safety Authority (EFSA) et al., 2018). It could be tempting to conclude that the 5 km pixels were too coarse to provide ecologically realistic simulations. Indeed, it is possible that a combination of the 5 km pixels, plus the low resolution (just three classes) land cover map, overly homogenized the landscape and therefore smoothed over potential landscape barriers (such as rivers) to ASF dissemination. Whilst a more realistic representation of WB ecology might be expected by adopting smaller pixels and a more detailed land cover map, our chosen approach struck a balance between ecological realism and computation time: smaller pixels risked making the numerical calculations too slow for meeting challenge deadlines. Moreover, our simulations did provide robust and accurate predictions of the epidemic's trajectory (see Fig. 2 in Ezanno et al. (2022)). Thus, the approach was appropriate for replicating ASF dissemination as simulated by the challenge organizers, and within the time frame of the challenge. However, a coarser resolution, or even a simplified (fewer transmission mechanisms) model, may be desirable if a fast response decision-making tool is required.

4.4.3. The role of WB carcasses

Climatic factors, and their effects on carcass longevity in the environment, are often cited as being important regarding the persistence of ASF transmission among WB. These factors have been shown to generate different patterns of ASF transmission and persistence among WB populations in (i) a North-Eastern European country (Estonia), compared to (ii) a Mediterranean country (Spain) (O'Neill et al., 2020). The effect of carcasses on ASF persistence is primarily driven by climatic factors, because the carcass decomposition rate is positively related to temperature. In our analyses, carcasses only played a very minor role in the rapid spread of ASF on Merry Island. This result is consistent with the hypothesized geographical location of Merry Island, where relatively stable daily maximum temperatures within a range of 16 and 25°C are expected all year long. Whilst our model does contain both live and carcass infection sources, it would need to be modified to include the effects of large seasonal temperature variations on carcass longevity for it to be useful in regions with long cold winters. Moreover, for the purposes of predicting persistence, it would also be useful to have more data on the movement patterns of WB (particularly young males) across areas depopulated by ASF.

4.4.4. Efficacy of fencing and hunting interventions

Within the challenge, both fencing and increased hunting were effective in limiting the impact of the first wave. However, the impact of fencing was compromised by a poor choice of location (considering the speed of disease spread) for the southern fence, which permitted the disease to leak south of the fence and buffer zone. This leaking reduced the contrast between data collected on either side of the fence, which likely resulted in a loss of statistical power that surely contributed to the large uncertainty in fence efficacy, and a potential underestimation of the benefits of fencing. As a result, it was hard to be conclusive about how effective fencing could have been had the western and southern fences been built earlier or placed further from the epicentre. Indeed, simulations with fence completion on day 30 (instead of day 60) provided a much more optimistic prospective for ASF elimination at day 230 (Fig. S5), Although the increased probability of elimination is largely due to extending the hunting period by 30 days, this does not explain the difference between trajectories at day 90 in Fig. S5 and day 120 in Fig. 6 - thus an earlier intervention would have greatly reduced the probability of a second wave. Finally, the large posterior uncertainty in fence efficacy also reflects our choice of a non-informative prior. An alternative prior in which a fully functional fence was more likely may have been more useful. However, ideally such a prior would be based on real data and not just subjective beliefs, and in the current context no such supplementary data were available.

4.4.5. Monte-Carlo synthetic likelihoods

A unique feature of our WB model was the use of Monte-Carlo simulation to approximate a likelihood, thereby permitting inference by MCMC. Our approach represents a variation of the classic approach to synthetic likelihood (Wood, 2010), which is also similar to approximate Bayesian computation (ABC) (Beaumont et al., 2002), in as much that inference is based on a set of summary statistics (of real and simulated data) - in our case, local 10-day aggregates of each observation type (active search, passive search, hunted). The key difference between our synthetic likelihood and the classic approach lies in the choice of distribution function — since we worked purely with aggregated counts, the Poisson distribution provided a natural discrete alternative to the multivariate-Gaussian classically used in synthetic likelihoods. Since these aggregated counts were evaluates within every pixel, and over various time intervals, they provided rich information for fitting the model, and further summary statistics were not required. The key advantage of using Monte Carlo to generate an approximate likelihood, for our stochastic spatial model, was that we could use NIMBLE's adaptive Metropolis–Hastings block sampler for exploring the posterior distribution (de Valpine and Paciorek, 2020). This algorithm was capable of detecting and adapting to strong correlations between model parameters — the strength of these correlations suggest that standard ABC would have suffered from very high rejection rates, unless an extremely generous acceptance threshold was adopted. Thus, we suggest that our approach did provide a more complete integration over the parameter space than could have been obtained via ABC. Another alternative to this Monte-Carlo likelihood would have been to use probability arguments from survival analysis, and expected values of I in the force of infection, in order to integrate analytically over uncertainty caused by event time censoring (Pleydell et al., 2018). However, whilst stochasticity within the Monte Carlo approach does add a degree of noise, it is easier, and arguably preferable, to base inference on the stochastic simulation of discrete events rather than to develop a continuous approximation via relatively complex probabilistic arguments.

4.4.6. The role of culling wild boar

A consistent assumption throughout the ASF Challenge has been that culling WB will not lead to changes in WB movement patterns. This might not be a serious simplification if a 100% effective fence entirely surrounds the affected area. However, in the ASF Challenge, the fence was presented as probably not being 100% effective and its location was a poor choice for preventing ASF spread to the west and (more importantly, given WB densities) south. A badly located fence, coupled with augmented dispersal of panicked WB is a combination of factors that could seriously diminishing the efficacy of control measures. Behavioural changes in response to culling can have important epidemiological consequences. Perhaps the best known example is that of badgers, culled in the UK during efforts to control bovine tuberculosis (bTB). The badgers increased their dispersal behaviour in response to culling, resulting in increases in bTB prevalence in and around cull areas (Donnelly et al., 2003; Pope et al., 2007; Woodroffe et al., 2006). The nature of behavioural changes in WB in response to culling is less well documented, although it seems likely that landscape effects could influence such changes. A recent review has highlighted numerous factors associated with culling wild animals which can negate the effects of disease control efforts (Miguel et al., 2020). Clearly more work is required in this area, so that ASF models can move beyond the simplest hypothesis of zero negative effects from culling WB. For these reasons, we urge that results from simple models are interpreted with caution and that control efforts are implemented with a margin of error.

4.5. Concluding remarks

The fictive scenarios emulated within the ASF Challenge present several similarities with recent real ASF incursions in European countries such as Belgium and the Czech Republic (Sauter-Louis et al., 2021), or Italy (IZSAM, 2022). In such scenarios, the majority of WB cases have remained clustered in one single infected area, after a point source introduction of unknown (but most likely human-mediated) origin. In both countries, the disease was successfully eradicated due to fast actions combining a diversity of measures, including containment with fences, active depopulation, zoning and passive surveillance (Jori et al., 2021). Our modelling has highlighted the importance of rapid and appropriate action in response to an outbreak, and has suggested that a combination of measures, possibly including active depopulation, may provide a successful strategy.

Funding

This research did not receive any specific grant from funding agencies in the public, commercial, or not-for-profit sectors.

CRediT authorship contribution statement

Facundo Muñoz: Conceptualization, Methodology, Software, Validation, Formal analysis, Data curation, Writing – original draft, Writing – review & editing, Visualization. **David R.J. Pleydell:** Conceptualization, Methodology, Software, Validation, Formal analysis, Data curation, Writing – original draft, Writing – review & editing, Visualization. **Ferrán Jori:** Conceptualization, Writing – original draft, Writing – review & editing, Project administration.

Declaration of competing interest

The authors declare that they have no known competing financial interests or personal relationships that could have appeared to influence the work reported in this paper.

Data availability

Data and code are available online. Links provided in the text.

Acknowledgements

We thank the ASFC organizers for their rigour and commitment to a interesting challenge. We also thank Mahé Liabeuf for discussions, analysis and insights regarding the behaviour of our WB model.

Appendix A. Supplementary material

Supplementary material related to this article can be found online at https://doi.org/10.1016/j.epidem.2022.100596.

References

Alexander, Neil Stewart, Massei, Giovanna, Wint, William, 2016. The European distribution of sus scrofa. Model outputs from the project described within the poster–where are all the boars? An attempt to gain a continental perspective. Open Health Data 4 (1).

Andrieu, Christophe, Doucet, Arnaud, Holenstein, Roman, 2010. Particle Markov chain monte carlo methods. J. R. Stat. Soc. Ser. B Stat. Methodol. 72 (3), 269–342.

Beaumont, Mark A., Zhang, Wenyang, Balding, David J., 2002. Approximate Bayesian computation in population genetics. Genetics 162 (4), 2025–2035.

Boklund, A., et al., 2020. Risk factors for African swine fever incursion in Romanian domestic farms during 2019. Sci. Rep. (ISSN: 2045-2322) 10 (1), 10215. http://dx.doi.org/10.1038/s41598-020-66381-3, https://pubmed.ncbi.nlm.nih.gov/32576841, https://www.ncbi.nlm.nih.gov/pmc/articles/PMC7311386/.

Bosch, J., et al., 2017. A cartographic tool for managing African swine fever in Eurasia: mapping wild boar distribution based on the quality of available habitats. Transbound. Emerg. Dis. 64 (6), 1720–1733.

Costard, S., et al., 2013. Epidemiology of African swine fever virus. Virus Res. 173 (1), 191–197.

de Valpine, P., Paciorek, C. others, 2020. NIMBLE: MCMC, particle filtering, and programmable hierarchical modeling. http://dx.doi.org/10.5281/zenodo.820703, URL: https://cran.r-project.org/package=nimble.

de Valpine, P., Turek, D. others, 2017. Programming with models: Writing statistical algorithms for general model structures with NIMBLE. J. Comput. Graph. Statist. 26, 403–417. http://dx.doi.org/10.1080/10618600.2016.1172487.

Devenish-Nelson, Eleanor S., et al., 2014. Demonstrating frequency-dependent transmission of sarcoptic mange in red foxes. Biol. Lett. 10 (10), 20140524.

Donnelly, Christl A., et al., 2003. Impact of localized badger culling on tuberculosis incidence in British cattle. Nature 426 (6968), 834–837.

European Food Safety Authority (EFSA), et al., 2018. Epidemiological analyses of African swine fever in the European union (November 2017 until November 2018). 16, (11), (ISSN: 18314732, 18314732) http://dx.doi.org/10.2903/j.efsa.2018.5494, URL: https://data.europa.eu/doi/10.2903/j.efsa.2018.5494,

Ezanno, Pauline, et al., 2022. The ASF modelling challenge: model comparison and lessons learnt. Epidemics (Under review).

Ferdousi, Tanvir, et al., 2019. Generation of swine movement network and analysis of efficient mitigation strategies for African swine fever virus. PLoS One 14 (12), e0225785. http://dx.doi.org/10.1371/journal.pone.0225785.

Gallardo, C., et al., 2017. Experimental infection of domestic pigs with African swine fever virus Lithuania 2014 Genotype II field isolate. 64, (1), (ISSN: 1865-1682) pp. 300–304. http://dx.doi.org/10.1111/tbed.12346, URL: https://onlinelibrary.wiley.com/doi/abs/10.1111/tbed.12346,

Gervasi, Vincenzo, Guberti, Vittorio, 2021. African swine fever endemic persistence in wild boar populations: Key mechanisms explored through modelling. 68, (5), (ISSN: 1865-1674, 1865-1682) pp. 2812–2825. http://dx.doi.org/10.1111/tbed.14194, URL: https://onlinelibrary.wiley.com/doi/10.1111/tbed.14194,

Gervasi, Vincenzo, Marcon, Andrea, et al., 2019. Evaluation of the efficiency of active and passive surveillance in the detection of African swine fever in wild boar. 7, (1), (ISSN: 2306-7381) p. 5. http://dx.doi.org/10.3390/vetsci7010005, URL: https://www.mdpi.com/2306-7381/7/1/5,

Gillespie, Daniel T., 2001. Approximate accelerated stochastic simulation of chemically reacting systems. J. Chem. Phys. 115 (4), 1716–1733.

Guinat, Claire, et al., 2016. Transmission routes of African swine fever virus to domestic pigs: Current knowledge and future research directions. Vet. Rec. 178 (11), 262–267.

Halasa, Tariq, et al., 2019. Simulation of transmission and persistence of African swine fever in wild boar in Denmark. Prevent. Vet. Med. (ISSN: 0167-5877) 167, 68–79. http://dx.doi.org/10.1016/j.prevetmed.2019.03.028, URL: https://www.sciencedirect.com/science/article/pii/S0167587718305944.

Hayes, Brandon H., et al., 2021. Mechanistic modelling of African swine fever: A systematic review. Prevent. Vet. Med. 105358.

IZSAM, 2022. Peste suina Africana nei selvatici. Zona infetta tra piemonte e liguria. Bollettino Epidemiologico Nazionale Veterinario URL: https://www.izs.it/BENV_NEW/Engine/RAServePG.php/P/1483710010500/M/309910040500/T/Peste-Suina-Africana-nei-selvatici-Zona-infetta-tra-Piemonte-e-Liguria.

Jori, F., Bastos, A.D.S., 2009. Role of wild suids in the epidemiology of African swine fever. EcoHealth 6 (2), 296–310.

Jori, F., et al., 2021. Management of wild boar populations in the European union before and during the ASF crisis.. In: Iacolina, L., Penrith, ML, Bellini, S., Chenais, E., Jori, F., Montoya, M., Ståhl, K., Gavier-Widén, D. (Eds.), Understanding and Combatting African Swine Fever. A European Perspective. Wageningen Academic Publishers, Wageningen, The Netherlands, pp. 197–228. http://dx.doi.org/10.3920/978-90-8686-910-7.

Landau, William Michael, 2018. The drake R package: A pipeline toolkit for reproducibility and high-performance computing. J. Open Source Softw. 3 (21).

Lange, Martin, Thulke, Hans-Hermann, 2017. Elucidating transmission parameters of African swine fever through wild boar carcasses by combining spatio-temporal notification data and agent-based modelling. Stoch. Environ. Res. Risk Assess. 31 (2), 379–391.

Lewis, Jesse S., et al., 2017. Biotic and abiotic factors predicting the global distribution and population density of an invasive large mammal. Sci. Rep. 7 (1), 1–12.

Mazur-Panasiuk, Natalia, Żmudzki, Jacek, Woźniakowski, Grzegorz, 2019. African swine fever virus–persistence in different environmental conditions and the possibility of its indirect transmission. J. Vet. Res. 63 (3), 303.

Mighell, Ellen, Ward, Michael P., 2021. African swine fever spread across Asia, 2018–2019. Transbound. Emerg. Dis..

Miguel, Eve, et al., 2020. A systemic approach to assess the potential and risks of wildlife culling for infectious disease control. Commun. Biol. 3 (1), 1–14.

OIE, 2021. African swine fever virus (Inf. with), Haiti. https://wahis.oie.int/#/report-info?reportId=39905. (Accessed 22 September 2021).

O'Neill, Xander, et al., 2020. Modelling the transmission and persistence of African swine fever in wild boar in contrasting European scenarios. Sci. Rep. 10 (1), 1–10.

Paulino-Ramirez, Robert, 2021. Food security and research agenda in African swine fever virus: A new arbovirus threat in the dominican Republic. InterAm. J. Med. Health 4.

Pebesma, Edzer J., Bivand, Roger S., 2005. Classes and methods for spatial data in R. R News 5 (2), 9–13, URL: https://CRAN.R-project.org/doc/Rnews/.

Penrith, Mary-Louise, 2009. African swine fever. Onderstepoort. J. Vet. Res. 76 (1), 91–95.

Pepin, Kim M., et al., 2020. Ecological drivers of African swine fever virus persistence in wild boar populations: insight for control. Ecol. Evol. 10 (6), 2846–2859.

Picault, Sébastien, et al., 2021. The African swine fever modelling challenge: objectives, model description and synthetic data generation. http://dx.doi.org/10.1101/2021.12.20.473417, BioRxiv, Cold Spring Harbor Laboratory.

Pittiglio, Claudia, Khomenko, Sergei, Beltran-Alcrudo, Daniel, 2018. Wild boar mapping using population-density statistics: From polygons to high resolution raster maps. PLoS One 13 (5), e0193295.

Pleydell, David R.J., et al., 2018. Estimation of the dispersal distances of an aphid-borne virus in a patchy landscape. PLoS Comput. Biol. 14 (4), e1006085.

Podgórski, Tomasz, Śmietanka, Krzysztof, 2018. Do wild boar movements drive the spread of African swine fever? 65, (6), (ISSN: 18651674) pp. 1588–1596. http://dx.doi.org/10.1111/tbed.12910, URL: https://onlinelibrary.wiley.com/doi/10.1111/tbed.12910,

Pope, Lisa C., et al., 2007. Genetic evidence that culling increases badger movement: Implications for the spread of bovine tuberculosis. Mol. Ecol. 16 (23), 4919–4929.

R. Core Team, 2020. R: A language and environment for statistical computing. R Foundation for Statistical Computing, Vienna, Austria, URL: https://www.R-project.org/.

Sales, Lilian Patrícia, et al., 2017. Niche conservatism and the invasive potential of the wild boar. J. Anim. Ecol. 86 (5), 1214–1223.

Sánchez-Vizcaíno, José Manuel, et al., 2019. African swine fever virus. Dis. Swine 443–452.

Sandra, Blome, Kati, Franzke, Martin, Beer, 2020. African swine fever–A review of current knowledge. Virus Res. 198099.

Sauter-Louis, Carola, et al., 2021. African swine fever: Why the situation in Germany is not comparable to that in the czech Republic or Belgium. Transbound. Emerg. Dis. (ISSN: 1865-1674) n/a (n/a), http://dx.doi.org/10.1111/tbed.14231, URL: https://onlinelibrary.wiley.com/doi/abs/10.1111/tbed.14231.

Taylor, Rachel A., et al., 2021. Predicting spread and effective control measures for African swine fever—Should we blame the boars? Transbound. Emerg. Dis. 68 (2), 397–416.

Tennekes, Martijn, 2018. Tmap: Thematic maps in R. J. Stat. Softw. 84 (6), 1–39. http://dx.doi.org/10.18637/jss.v084.i06.

Viltrop, A., et al., 2021. African swine fever epidemiology, surveillance and contro. In: Iacolina, L., Penrith, M.L., Bellini, S., Chenais, E., Jori, F., Montoya, M., Ståhl, K., Gavier-Widén, D. (Eds.), Understanding and Combatting African Swine Fever. A European Perspective. Wageningen Academic Publishers, Wageningen, The Netherlands, pp. 229–261.

Volkova, Victoriya V., et al., 2010. Sheep movement networks and the transmission of infectious diseases. In: Galvani, Alison P. (Ed.), PLoS One (ISSN: 1932-6203) e11185. http://dx.doi.org/10.1371/journal.pone.0011185, 5 (6) URL: https://dx.plos.org/10.1371/journal.pone.0011185.

Wood, Simon N., 2010. Statistical inference for noisy nonlinear ecological dynamic systems. Nature 466 (7310), 1102–1104.

Woodroffe, Rosie, et al., 2006. Culling and cattle controls influence tuberculosis risk for badgers. Proc. Natl. Acad. Sci. 103 (40), 14713–14717.

Xie, Yihui, 2020. Knitr: A general-purpose package for dynamic report generation in R. URL: https://yihui.org/knitr/, R package version 1.30.